ENVIRONMENTAL RESEARCH
LETTERS

Diurnal and seasonal patterns of global urban dry islands

To cite this article before publication: Naika Meili *et al* 2022 *Environ. Res. Lett.* in press https://doi.org/10.1088/1748-9326/ac68f8

Diurnal and Seasonal Patterns of Global Urban Dry Islands

Naika Meili[1], Athanasios Paschalis[2], Gabriele Manoli[3], Simone Fatichi[1]

[1]Department of Civil & Environmental Engineering, National University of Singapore, Singapore
[2]Department of Civil & Environmental Engineering, Imperial College London, UK
[3]Department of Civil, Environmental & Geomatic Engineering, University College London, UK

Abstract

Urban heat islands (UHIs) are a widely studied phenomenon, however, research on urban-rural differences in humidity, so called urban dry or moisture islands (UDIs, UMIs), is less common and a large-scale quantification of the seasonal and diurnal patterns of the UDI effect is still lacking. Quantification of the UDI/UMI effect is essential to understand the impacts of humidity on outdoor thermal comfort, building energy consumption, and urban ecology in cities worldwide. Here, we use a set of globally distributed air temperature and humidity measurements (1089 stations) to quantify diurnal and seasonal patterns of UHI and UDI resulting from rapid urbanization over many regions of the world. The terms “absolute UDI” and “relative UDI” are defined, which quantify urban-rural differences in actual and relative humidity measurements, respectively.

Results show that absolute UDI is largest during daytime with the peak humidity decrease in urban areas occurring during late afternoon hours. In contrast, relative UDI is largest during night and the peak urban relative humidity decrease occurs in the late evening hours with values around -10 to -11% for relative humidity and 2.9 to 3.6 hPa for vapor pressure deficit between 20 – 00 local time during summer. Relative and absolute UDIs are largest during the warm season, except for daytime relative humidity UDI, which does not show any seasonal pattern. In agreement with literature, canopy air UHI is shown to be a nighttime phenomenon, which is larger during summer than winter. Relative UDI is predominantly caused by changes in actual humidity during day and UHI during nighttime.

Social media abstract:

Diurnal and seasonal patterns of absolute and relative urban dry islands at the global scale

Key words: urban dry island, urban moisture island, urban heat island, urban climate, urbanization effects, humidity

1. Introduction

Cities are growing in size and 60% of the world's population is projected to live in urban areas by 2030 (United Nations, 2018). At the same time, cities have been found to exhibit distinct climate features with alterations of temperature and humidity causing urban heat or cool islands (UHIs or UCIs) and urban dry or moisture islands (UDIs or UMIs) (Du et al., 2022; Y. Li et al., 2020; Lokoshchenko, 2017; Luo & Lau, 2019; Manoli et al., 2019; Zhao et al., 2014).

These changes in local climate caused by urbanization can potentially impact human well-being and health (Mora et al., 2017; Tuholske et al., 2021; X. Wang & Gong, 2010), as changes in temperature and humidity both affect human outdoor thermal comfort. For example, rural irrigation has been shown to increase moist heat stress extremes in India (Mishra et al., 2020), while a decrease in humidity in Beijing could partially offset the anticipated increase in heat stress caused by higher temperatures (X. Wang & Gong, 2010). Changes in humidity also affect plant stomatal response and evapotranspiration, which could impact urban ecology (Chen et al., 2011; Gillner et al., 2017; Novick et al., 2016). Furthermore, temperature and humidity influence the energy consumption for building cooling and heating (Fonseca & Schlueter, 2020; Maia-Silva et al., 2020; Santamouris, 2014). For example, Fonseca & Schlueter (2020) predict an increase in energy usage for building cooling in hot and humid cities due to higher needs for dehumidification, which indicates not just the role of temperature but also humidity differences on the energy consumption of cities (Maia-Silva et al., 2020).

While there is a wealth of literature focusing on UHI (e.g., Oke et al., 2017; Venter et al., 2021), especially from the surface temperature perspective (X. Li et al., 2016; Manoli et al., 2019, 2020a; Paschalis et al., 2021; Peng et al., 2011; C. Wang et al., 2016; Ward et al., 2016; Zhou et al., 2013), studies analyzing humidity changes in cities are scarce. Available studies on urban humidity focus on single cities (e.g. Ackerman, 1987; Cuadrat et al., 2015; Fortuniak et al., 2006; Hage, 1975; Lokoshchenko, 2017; Z. Wang et al., 2021; Yang et al., 2017) or specific urbanized regions (Hao et al., 2018; Luo & Lau, 2019). A comprehensive analysis of the causes for the formation of UDIs and UMIs, as well as their diurnal and seasonal patterns globally is still lacking.

Studies also vary in the analyzed and reported humidity metrics, which further limits the potential for comparison and leads to large differences in the reported urban humidity effects. For example, several studies report lower humidity in cities and hence, an urban dry island (UDI) (e.g. Cuadrat et al., 2015; Hao et al., 2018; Luo & Lau, 2019; Moriwaki et al., 2013; Tapper, 1990; Yang et al., 2017), while other authors report an higher air moisture in cities and argue for the presence of an urban moisture island (UMI) (e.g. Ackerman, 1987; Lee, 1991; Tapper, 1990; Z. Wang et al., 2021). These contrasts could be caused by urban specific differences, anthropogenic water sources (e.g., Huang et al., 2021), absent or delayed dewfall due to higher temperatures and different surface materials (e.g., Kuttler et al., 2007), or regional moisture transport (e.g., Du et al., 2022). However, they are likely also due to differences in the analyzed humidity metrics and their variability on seasonal and diurnal timescales.

Humidity in the air can be assessed with metrics specifying the actual water content in the air, such as absolute water vapor density (g/m3), specific humidity (q, g/kg), and vapor pressure (e, hPa), or with metrics specifying the relative humidity level in the air in relation to its saturation point at a given temperature (e.g. saturated vapor pressure, e_{sat}), such as relative humidity ($RH \approx 100*e/e_{sat}$, %) or vapor pressure deficit ($VPD = e_{sat}-e$, hPa) (e.g. Shuttleworth, 2012). Values of relative humidity metrics (RH, VPD) can change due to a difference in temperature alone without any change in the amount of water vapor in the air. For example as warmer air can hold more moisture, e_{sat} and consequently VPD increase (e.g. Shuttleworth, 2012). On the other hand, higher air temperatures (T_{air}) can also lead to

an increase in actual humidity (i.e., q and e) if there are no limitations to the moisture supply and its transport from the land surface to the air or through advection from adjacent regions (e.g., Du et al., 2022). However, during urban development, vegetated and pervious areas are often converted to impervious surfaces, which can strongly limit water supply from the land to the atmosphere due to suppression of evapotranspiration. Therefore, changes in humidity in cities, observed as UDI or UMI, can be caused by a change in T_{air} and/or a change in the actual humidity. This has already been shown in some studies attributing the observed UDI or UMI to changes in T_{air} (e.g. Lokoshchenko, 2017) or evapotranspiration (e.g. Hao et al., 2018). However, a general analysis of the relative contribution of temperature (i.e., UHI) and moisture content on UDI and UMI throughout the diurnal and seasonal cycles is still lacking. A clearer distinction between UDI and UMI based on actual or relative humidity metrics is needed to synthesize and generalize urbanization effects on atmospheric humidity.

Availability of measurements with high spatial coverage across a city and its surroundings (e.g. Warren et al., 2016), which is commonly used to quantify UHI, is scarce and limits large-scale studies of near ground (often referred to as canopy) UHI and UDI across different cities and climates. To overcome this limitation, recent studies have employed crowd-sourced meteorological measurements to quantify the UHI effect across multiple cities (Venter et al., 2021), but such attempts are still rare. Here, we take an alternative approach, proposing a space for time substitution, and leverage the fact that many regions of the world experienced urbanization in the last few decades, likely increasing their UHI and UDI. Hence, we correlate urbanization rate with trends in T_{air} and humidity (q, e, RH, VPD) using a large number (1089) of globally distributed meteorological stations (J. H. R. Dunn et al., 2012; 2016; 2019; Smith et al., 2011), out of which 590 experience urbanization in their surroundings larger than 1% per decade. The proposed methodology also separates UHI and UDI from climate change effects. We quantify the seasonal and diurnal patterns of UHI, and "relative" and "absolute" UDI to distinguish between humidity differences in cities quantified by actual and relative humidity metrics. We further partition and attribute relative UDI magnitudes, measured in VPD, to changes in temperature and actual moisture distinguishing seasons and hours of the day.

Specifically, we answer the following research questions: What is the typical average diurnal and seasonal pattern of UDIs at the global scale and are there differences for relative and absolute UDI? Are there differences in the diurnal and seasonal patterns of relative and absolute UDI? To what extent is relative UDI caused by changes in temperature and to what extent by changes in actual moisture in the air? We finally discuss the potential impacts of urban humidity changes on outdoor thermal comfort, building energy usage, and urban ecology.

2. Methods

2.1 Meteorological observation data of humidity and air temperature

This study uses sub-daily meteorological observations of air and dew point temperature (T_{air}, T_{dew}) from HadISD version 3.1.1.2020f (Dunn et al., 2012; 2016; 2019; Smith et al., 2011). The HadISD data set is a subset of the Integrated Surface Database (ISD) of NOAA's National Climatic Data Center (Moustakis et al., 2020, 2021; Smith et al., 2011) and is synthesized by the Met Office Hadley Centre through the application of additional data quality processes and criteria on data availability. Relative humidity (RH), specific humidity (q), vapor pressure (e), and vapor pressure deficit (VPD) are calculated as a function of T_{air} and T_{dew} (SI Table 1).

The raw data set contains 8258 stations with at least partial data coverage during the analyzed time period of 1st of January 1990 to 31st of December 2018 (29 years). The raw meteorological time series

of the HadISD data set are not formally homogenized. However, a homogeneity assessment, including the time and magnitude of break points for affected stations, is available and provided by Dunn et al. (2014). The final set of stations used in this study is selected based on low inhomogeneity magnitudes of breakpoints as well as continuous data availability to compute the diurnal and seasonal cycles. The station selection criteria and data processing are outlined in detail in the supplementary information together with a methodological workflow figure (SI Sect. 1, SI Figure 1). The final data set comprises a total of 1089 stations with most of the stations located in the northern mid-latitudes (Figure 1). For the further analysis, average diurnal cycles of T_{air} and humidity variables (q, e, RH, VPD) are calculated for each month in each year for each station. In the following, we will refer to this as YMH_Si data average (SI Figure 1).

2.2 Background climate data from reanalysis and gridded products

Urbanization and climatic trends have co-occurred in the last decades, and both are not evenly distributed over the globe. The correlation of urbanization rate with change in temperature and humidity as done in our study (see Sect. 2.4) could lead to a result, which is not caused by the process of urbanization itself but purely by an artifact of certain climatic trends occurring (or not) in regions experiencing urbanization. Therefore, we use the ERA5 reanalysis product (Hersbach et al., 2020), which was bias corrected and aggregated to 0.5° resolution by Cucchi et al. 2020 (Climate Data Store, 2020) to check for such a co-linearity between trends in background climate and urbanization rate. The land surface scheme used to develop the ERA5 product does not currently include urbanization effects (Balsamo et al., 2009; Bassett et al., 2021; Hogan et al., 2017; Venter et al., 2021) and it has been successfully used in previous studies to represent the rural baseline climate (e.g, Bassett et al., 2021; Venter et al., 2021). The hourly ERA5 data was aggregated identically to the YMH_Si data averages, which includes the calculation of the average diurnal cycle of the meteorological variables for each station for each month in each year.

2.3 Impervious area and urbanization rate

We extract the percentage of artificial impervious area within a buffer radius of 7 km from each selected meteorological stations from an annual data set of Global Artificial Impervious Areas (GAIA) at 30 m resolution (Gong et al., 2020, downloaded from http://data.ess.tsinghua.edu.cn, 22nd of March 2021). The GAIA data set is based on 30-m resolution Landsat images and spans the years 1985-2018. The early years of the data set contain larger uncertainties due to limited data availability (Gong et al., 2020). Hence, only the years 1990-2018 (29 years) are used in this study. To determine the appropriate size of the extraction radius, the urbanization rate Δimp around each meteorological station was first calculated with different buffer radii ranging from 1 – 30 km and their correlation with the trends in air temperature and humidity was analyzed for day and nighttime separately during the summer months (June, July, August). The correlation coefficients tend to stabilize between an extraction radius of 6 – 9 km (SI Figure 2) and any of these radii are an acceptable choice for this study. A radius of 7 km was finally chosen for the impervious landcover extraction, which also corresponds to the value used by Luo & Lau, (2019). Note that the results presented here were also derived with other extraction radii to confirm that the diurnal and seasonal patterns shown in this study are independent of the exact extraction radius for radii ranging from 2 – 9 km. The magnitude of the calculated UHI and UDI is, however, dependent on the chosen extraction radius as urbanization rates Δimp tend to decrease with increasing analyzed area and thus radius (SI Figure 3). Diurnal and seasonal patterns of UHI and UDI calculated for a 4 km and 9 km buffer radius are shown in the supplementary information for comparison (SI Figure 4 – 7). The urbanization rate Δimp (fraction / decade) is calculated as the linear trend of impervious landcover within the chosen buffer radius from each station over the 29 analyzed years (1990-2018) (Luo & Lau, 2019). The majority of the urbanizing

stations show a fairly linear urbanization trend (SI Figure 8). Of the 1089 stations, 590 experience an artificial impervious land conversion rate larger than 1% per decade within the 7 km buffer radius while 499 experience no or negligible urbanization. Spatial distribution of non-urbanizing and urbanizing stations, including their urbanization rates, is shown in figure 1. Note, that some station with a small urbanization rate can still be surrounded by urban areas, which developed before 1990. However, there is only a small number of stations for which this is the case. There are 7 stations with an artificial impervious land cover of more than 10 % in 1990 and an urbanization rate of less than 1 % per decade.

2.4 Urban Dry Island (UDI) and Urban Heat Island (UHI) calculation

UDI and UHI are traditionally calculated as the difference of humidity and temperature measured within an urban area and at a rural reference station (Oke et al., 2017) and measurements need to be obtained simultaneously in multiple locations within and around a city. However, such simultaneous meteorological measurements within cities and their rural surroundings are limited to a few sites with dense meteorological networks or dedicated measurement campaigns but are lacking at the global scale. In this study, we take an alternative approach to overcome this limitation by focusing on temporal differences in landcover as proposed by Luo & Lau (2019). During the process of urbanization, natural landcover is replaced by urban infrastructure leading to the development of UDI and UHI over time. Meteorological measurements at fixed locations experiencing urbanization in their surroundings are likely measuring trends in temperature and humidity, which differ from trends at rural and non-urbanizing stations nearby and are associated with this landcover change. Following this reasoning, we correlate trends in humidity and temperature measured at the 1089 HadISD stations with their urbanization rates (Δimp) over the analyzed 29-year time period to obtain magnitudes of UDI and UHI (Figure 2). Trends in humidity (ΔRH, ΔVPD, Δe, Δq) and air temperature (ΔT_{air}) are calculated for each station, urbanizing and non-urbanizing, as the linear trend over the 29-year time period (1990-2018). Climatic trends derived for rural HadISD stations are likely associated to climate change, while climatic trends in urbanizing areas include both climate change as well as urbanization effects in the HadISD data set. Monthly ERA5 trends for each station are subtracted from the monthly HadISD trends. By means of this correction, we remove any climate change signal and any trends resulting from a co-linearity between background climate trends and urbanization rate, and we focus only on urbanization effects as further explained in the supplementary information (SI Sect. 2, SI Figure 1, 9 – 13).

Magnitudes of UDI and UHI and climate change effects can be derived from the slope and intercept parameters of the linear regression between urbanization rate (Δimp) and climate trends (ΔRH, ΔVPD, Δe, Δq, ΔT_{air}) as shown here for the example of T_{air}: $\Delta T_{air} = S_{urb} * \Delta imp + CC$. The slope S_{urb} is the UHI magnitude, which is expected to develop if a location experiences complete urbanization starting from rural conditions (i.e., an increase from 0 to 100% of artificial impervious areas within a radius of 7 km from the station). The linear regression in Figure 2 shows an intercept (CC) close to 0 as the average climate change effects are removed with the ERA5 correction. Statistical significance of UDI and UHI magnitudes are determined by means of a two-sided t-test at the 5% significance level (i.e., $p<0.05$ indicating a slope S_{urb} different than zero).

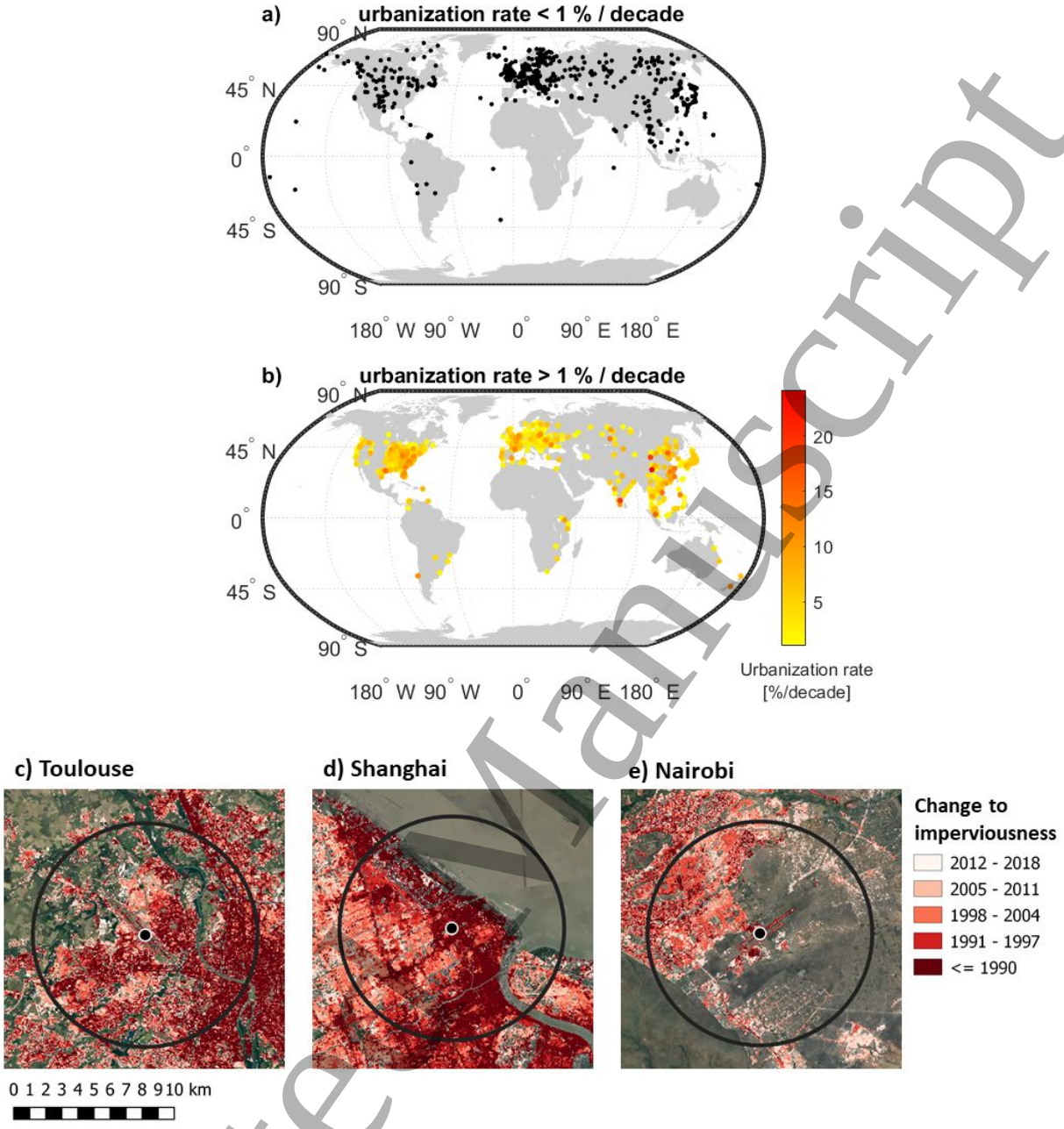

Figure 1: Location of meteorological stations: a) stations with less than 1% increase in artificial impervious landcover per decade and b) urbanizing locations with more than 1% increase in artificial impervious landcover per decade within a radius of 7 km. c), d), e) Impervious land cover change over time within a radius of 7 km (black circle) from meteorological stations (black point) in the urban area of Toulouse in France, Shanghai in China, and Nairobi in Kenya as examples of the extracted impervious landcover change.

UDI and UHI magnitudes shown in Figure 3 to 5 correspond to the slope of the linear regression for each season and hour of the day. Winter comprises the months December to February (June to August), spring the months March to May (September to November), summer the months June to August (December to February), and autumn the months September to November (March to May) for the northern (southern) hemisphere. Daytime includes the hours from 7 to 18 local time (LT) and nighttime the hours 19 - 6 LT. As most of the stations are located in the northern hemisphere, Figure 3 - 5 display the northern hemisphere months of the seasonal UDI and UHI effects. However, the southern hemisphere stations are also included in the displayed results in Figure 3 - 5 with the

appropriate correction (i.e. the southern hemisphere month January is included in the results for the northern hemisphere month July and so forth).

To analyze differences in UDI according to the aridity level of the background climate, we split the dataset into stations with wetness index WI<1 and WI>1, corresponding to climates, in which evapotranspiration is water or energy limited, respectively. The wetness index (WI) is calculated as the ratio between mean annual precipitation and mean annual potential evapotranspiration (WI=P/PET) and the corresponding data is extracted from the Climatic Research Unit gridded Time Series (CRUTS4.05) data set (Harris et al., 2020).

Note that positive UHI values denote higher T_{air} in urban areas compared to natural land surfaces. Less humidity in cities is shown by negative UDI_q, negative UDI_e, negative UDI_{RH}, and positive UDI_{VPD}. For the following discussion, we introduce the terms “absolute UDI” and “relative UDI”. Absolute UDI includes UDI_q and UDI_e, which specify the change in actual water content in the air. Relative UDI comprises UDI_{RH} and UDI_{VPD}. Relative humidity measures can change due to a change in T_{air} alone, e.g. caused by UHI, without a change in actual humidity.

2.5 Attribution of UDI effects to changes in temperature and changes in vapor supply

Observed changes in humidity in cities can be attributed to changes in T_{air} caused by UHI and changes in humidity supply because of the increase in artificial impervious area, leading to reduced water availability for evapotranspiration. To separate these two causes, we partition the measured UDI_{VPD} ($\delta VPD/ \delta imp$) into changes associated to an increase in e_{sat} caused by the UHI ($de_{sat}/dT_{air} * \delta T_{air}/ \delta imp$) and to a change in e ($\delta e/ \delta imp$):

$$\frac{\delta VPD}{\delta imp} = \frac{de_{sat}}{dT_{air}} \frac{\delta T_{air}}{\delta imp} - \frac{\delta e}{\delta imp}$$

where d and δ denote path-independent (exact) and path-dependent (inexact) differential operators. e_{sat} is calculated as a function of the measured temperature according to SI Table 1.

3. Results

3.1 Annual average UDI and UHI

We find a statistically significant UDI at the annual scale for both absolute and relative humidity measures. Annual average RH decreases by 4.8%, VPD increases by 1.22 hPa, e decreases by 0.78 hPa, and q decreases by 0.5 g/kg with a full replacement of natural landcover by artificial impervious areas within a radius of 7 km from the meteorological stations (Figure 2, SI Figure 14). The changes in annual average T_{air} due to the increase in impervious area from 0 to 100 % is +0.23°C and not statistically significant with a p-value of 0.094 (t-test for zero slope, Figure 2), indicating that the UHI effect is not apparent on the annual average based on the current data set and methodology. Note, that while a UHI magnitude of +0.23°C at a full replacement of natural landcover seems small, this number represents the annual average UHI, including all weather conditions, hours of the day and seasons. At the diurnal and seasonal scale, larger UHI intensities are found (see Sect. 3.2) with magnitudes similar to the ones reported by other large scale studies (e.g.,Venter et al., 2021).

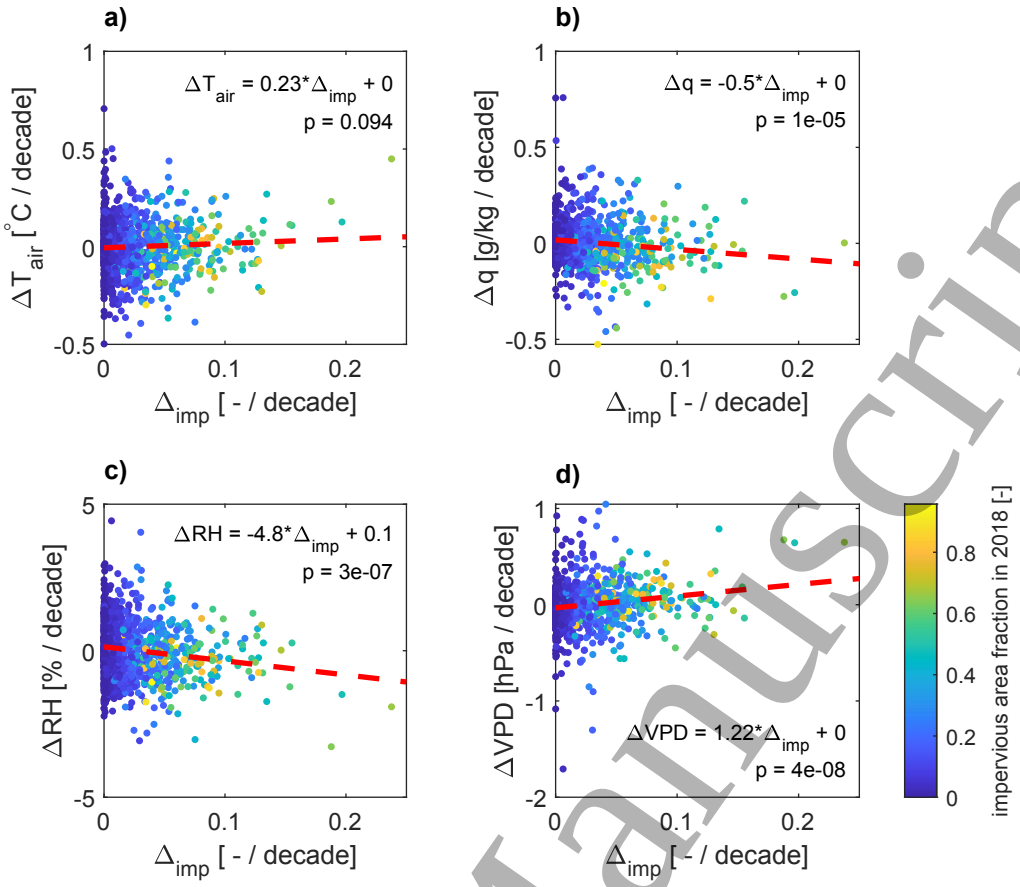

Figure 2: Changes in mean annual air temperature (ΔT_{air}) and humidity metrics (Δq, ΔRH, ΔVPD) with increase in artificial impervious land cover (Δimp) within a 7 km radius from each station. The slope of the fitted linear regression (red dotted line & displayed equation) quantifies the change in T_{air}, q, RH, and VPD associated with an artificial impervious land cover increase from 0 to 100%. We refer to this as the UHI and UDI magnitude in the following. p indicates the p-values of the correlation and is used to assess the statistical significance.

3.2 Diurnal and seasonal patterns of UDI and UHI

While there is no statistically significant UHI detected at the annual scale at a significance level of 0.05 (Sect. 3.1), we recover the typical diurnal pattern of UHI, with higher T_{air} at night and negligible UHI during daytime (Oke et al., 2017; Venter et al., 2021). The nighttime UHI is largest during the warm period of the year with a magnitude of 0.5-1.4 °C from April to September (October to March) in the northern (southern) hemisphere and negligible during winter. The same seasonal pattern is also observed in large scale studies quantifying surface UHI throughout the year (Manoli et al., 2020b; Paschalis et al., 2021; Zhou et al., 2013). The UHI effect is not detected during daytime throughout the year (Figure 3 and 4).

The absolute UDI is largest during the warm period (from May to September and November to March in the northern and southern hemisphere, respectively) ranging from -0.9 to -1.1 g/kg and -1.4 to -1.7 hPa during day and -0.4 to -0.75 g/kg and -0.6 to -1.2 hPa during nighttime for UDI_q and UDI_e, respectively. Statistically significant UDI_q and UDI_e are also detected during some winter months but with a smaller magnitude (Figure 3 and 4). Absolute UDI is largest during the daytime and in the early evening hours reaching a peak of -1.4 g/kg and -2.1 to -2.2 hPa from 17-19 h LT in summer for UDI_q and UDI_e, respectively. Absolute UDI is minimal from midnight to the early morning hours or even noon, depending on the season (Figure 3 and 4, SI Figure 15).

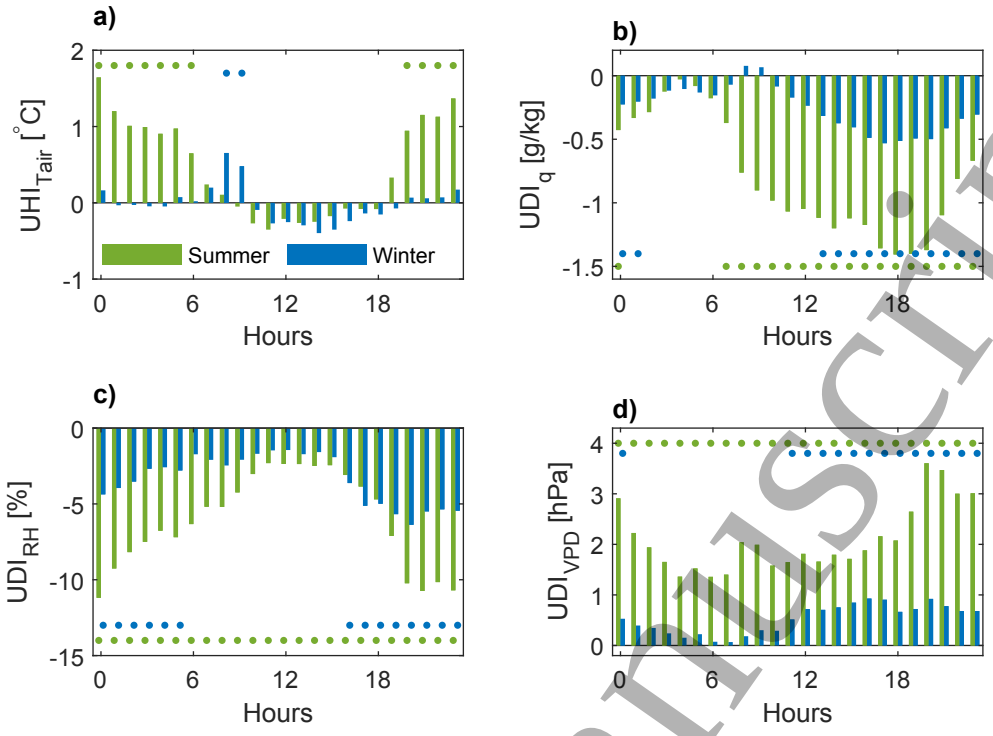

Figure 3: Average diurnal patterns of UHI and UDI computed with all stations: a) T_{air}, b) q, c) RH, and d) VPD for summer and winter months. UHI and UDI magnitudes are the expected change in air temperature and humidity variables with a full landcover conversion from natural to 100% artificial impervious surfaces within a radius of 7 km of the meteorological stations. The points indicate statistically significant UHI and UDI magnitudes with a p-value smaller than 0.05. Positive UHI_{Tair} denotes higher air temperature in cities compared with their rural surroundings. Negative UDI_q, negative UDI_{RH}, and positive UDI_{VPD} denote lower humidity in cities compared with their rural surroundings.

In contrast, relative UDI magnitudes are larger during night compared to daytime. Peak values range from -10 to -11% and 2.9 to 3.6 hPa between 20-00 LT during summer for UDI_{RH} and UDI_{VPD}, respectively. Diurnal differences of relative UDI magnitudes are larger for UDI_{RH} than for UDI_{VPD}. UDI_{VPD} is largest during the warm season ranging from 1.4 to 2 hPa and 1.6 to 2.7 hPa during May to September for day and nighttime, respectively. Similarly, nighttime UDI_{RH} shows a distinct seasonal cycle with larger nighttime UDI_{RH} values during the warm period (-8 to -10% from May to September). Daytime UDI_{RH} is smaller and does not show a distinct seasonal pattern.

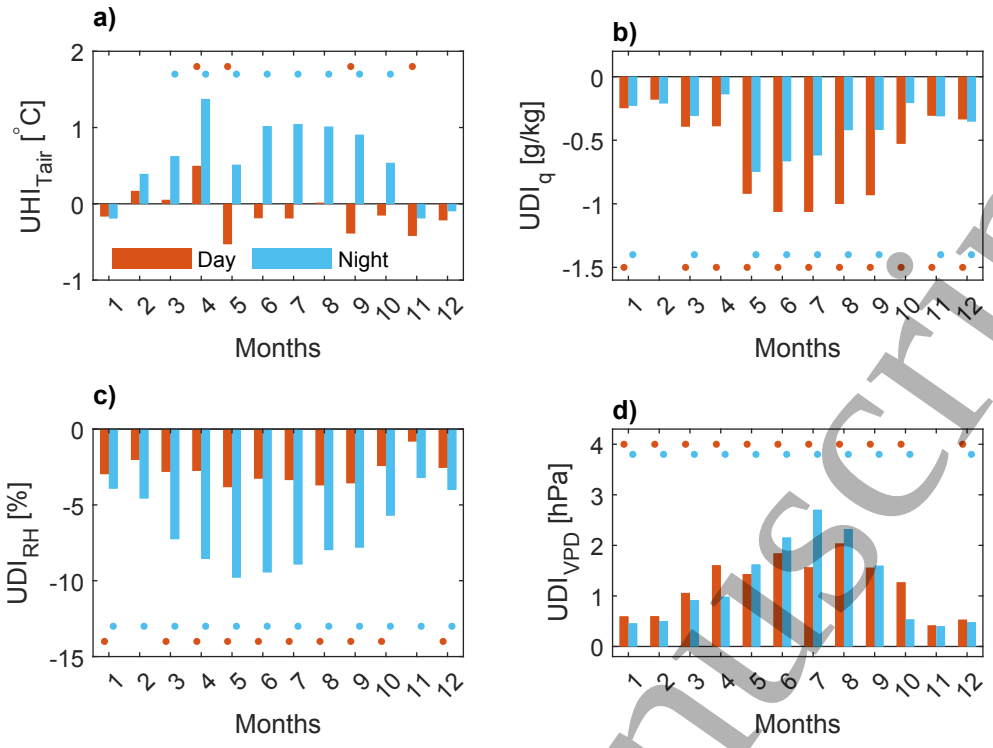

Figure 4: Average seasonal patterns of UHI and UDI computed with all stations: a) T_{air}, b) q, c) RH, and d) VPD for day- and nighttime. UHI and UDI magnitudes are the expected change in air temperature and humidity variables with a full landcover conversion from natural to 100% artificial impervious surfaces within a radius of 7 km of the meteorological stations. The points indicate statistically significant UHI and UDI magnitudes with a p-value smaller than 0.05. Positive UHI_{Tair} denotes higher air temperature in cities compared with their rural surroundings. Negative UDI_q, negative UDI_{RH}, and positive UDI_{VPD} denote lower humidity in cities compared with their rural surroundings.

In summary, absolute UDI is largest during the warm season and daytime with a peak in the late afternoon and early evening hours. Relative UDI is largest during the warm season and at nighttime with a peak in the late evening hours. Diurnal differences are more distinct for UDI_{RH} than for UDI_{VPD} and daytime UDI_{RH} does not show a strong seasonal dependence.

The separation of stations using WI<1 and WI>1 showed a larger absolute and relative UDI for wet climates during summer and daytime (SI Figure 16). However, the results are dependent on the selected WI cut-off point (Sect. 2.4). Hence, the here reported differences of UDI with WI are deemed not robust and require larger datasets to be fully analyzed.

3.3 Attribution of UDI_{VPD} effects to changes in T_{air} and changes in e

Relative UDI, here shown using UDI_{VPD}, are partly caused by UDI_e and UHI, which leads to an increase in e_{sat}. Partitioning of UDI_{VPD} shows that both, UHI and UDI_e, have a substantial contribution to the overall UDI_{VPD} during the warm season. Following the diurnal patterns of UHI and UDI_e, UDI_{VPD} is largely caused by UDI_e during daytime and by UHI from midnight to the early morning hours during summer (Figure 5a). During the late evening hours in summer, UDI_{VPD} is caused by both UHI and UDI_e in roughly equal magnitude leading to peak values of UDI_{VPD} during this time. Due to the absence of a significant UHI, wintertime UDI_{VPD} is almost only caused by UDI_e and is much smaller in magnitude (Figure 5c).

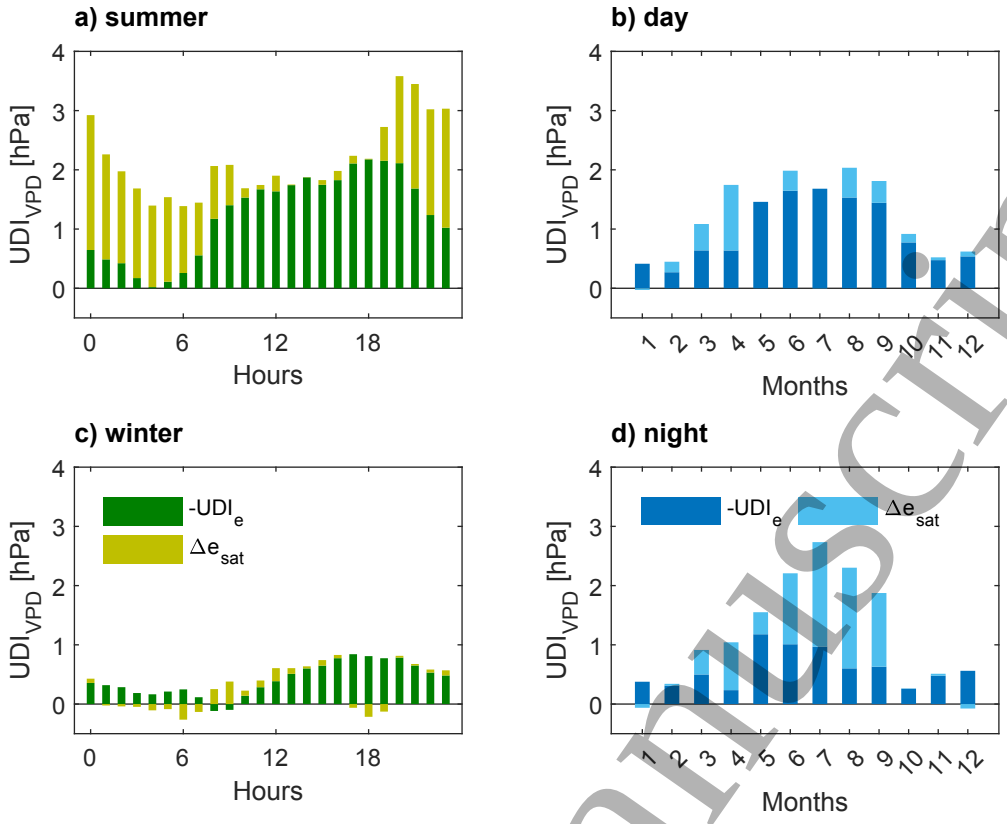

Figure 5: Partitioning of diurnal and seasonal patterns of UDI_{VPD} into changes associated to an increase in e_{sat} caused by UHI (Δe_{sat} is calculated as a function of ΔT_{air}) and to a change in e (UDI_e) for a) summer, b) daytime, c) winter, and d) nighttime. Positive UDI_{VPD} denotes lower humidity in cities compared to their rural surroundings. Note, that $-UDI_e$ is displayed in this graph instead of UDI_e as negative values of UDI_e denote lower humidity in cities compared with their rural surroundings.

4. Discussion

4.1 Reconciliation of UDI differences in literature through the separation of absolute and relative UDI

Current UDI literature, based on the analysis of single cities (e.g. Cuadrat et al., 2015; Lokoshchenko, 2017; Yang et al., 2017) or urbanized regions (e.g. Hao et al., 2018; Luo & Lau, 2019), reported diverging findings, ranging from a drier urban environment, i.e., UDI (e.g. Luo & Lau, 2019; Moriwaki et al., 2013), to air with higher moisture content in cities and thus a UMI (e.g. Lee, 1991; Z. Wang et al., 2021). While parts of these differences are likely caused by site specific environmental conditions, such as anthropogenic water sources (e.g., Huang et al., 2021; Wang et al., 2021) or regional moisture transport (e.g., Du et al., 2022), the distinction between relative and absolute UDI, which are assessed by relative humidity metrics (RH, VPD) and by metrics specifying the absolute water content in the air (e, q, absolute humidity), respectively, plays an important role in the reported differences. Furthermore, UDIs show a distinct seasonal and diurnal cycle (Figure 3 and 4), which can also lead to the presence or absence of UDI, depending on the period of investigation. Our large-scale study, quantifying the diurnal and seasonal patterns of relative and absolute UDI, can generalize the UDI behavior for the first time at the global scale.

When analyzing urban-rural differences in relative humidity measures, such as RH and VPD, results agree amongst different studies. Relative UDI has been reported in cities around the globe with various background climates such as Beijing (Yang et al., 2017) and the urban agglomerate of the

Yangtze River Delta in China (Hao et al., 2018; Luo & Lau, 2019), Zaragoza in Spain (Cuadrat et al., 2015), Moscow in Russia (Lokoshchenko, 2017), Berlin in Germany (Langendijk et al., 2019), Lodz in Poland (Fortuniak et al., 2006), Chicago in the USA (Ackerman, 1987), and Edmonton in Canada (Hage, 1975). The results of our large-scale analysis confirm and generalize these results by showing higher relative UDI during night compared to daytime (e.g. Yang et al., 2017) and during the warm compared to the cold season (e.g. Langendijk et al., 2019; Luo & Lau, 2019).

However, literature results start to diverge when assessing absolute UDI, with studies showing both the presence of UDI (e.g. Luo & Lau, 2019; Moriwaki et al., 2013) and UMI (e.g. Lee, 1991; Z. Wang et al., 2021). The occurrence of either UDI or UMI is dependent on time of the day and season. Absolute UDI was found mostly during daytime and summer (Hage, 1975; Lee, 1991; Moriwaki et al., 2013; Tapper, 1990), while UMI is mostly reported at night and during winter (Hage, 1975; Lee, 1991; Tapper, 1990) except for a study focusing on Hong Kong (Z. Wang et al., 2021), which has a strong UMI likely caused by substantial anthropogenic moisture sources in the city (Huang et al., 2021) and regional moisture transport (Du et al., 2022). While our large-scale analysis does not find a significant UMI, the same distinct diurnal pattern is shown with the largest absolute UDI during daytime and a small to non-existent absolute UDI at night. At the seasonal time-scale, our results also generalize previous results showing higher values of UDI during the warm season compared to winter (e.g. Luo & Lau, 2019; Moriwaki et al., 2013).

Warmer air, as caused by the UHI, increases e_{sat} and can cause relative UDI with a minimal change in absolute moisture in the air as shown for nighttime conditions. However, warmer air is also capable to hold more moisture in the absence of water supply limitations (e.g. Shuttleworth, 2012). Hence, UHI might cause absolute UMI as reported in some studies (Hage, 1975; Lee, 1991; Tapper, 1990) if ample moisture is available due to local moisture sources and evapotranspiration (Huang et al., 2021), or lateral advection of moisture (Du et al., 2022). Higher temperatures in cities and different surface properties can also lead to the absence or a delayed dewfall causing an absolute UMI (Kuttler et al., 2007). Due to the higher water holding capacity of warmer air, a small absolute UDI in correspondence with considerable UHI does not necessarily indicate that impervious land cover does not influence local atmospheric moisture, but simply that UHI partially offsets absolute UDI. This is shown by the presence of a high relative UDI as seen in this study at night and also often reported in literature (e.g. Cuadrat et al., 2015; Hao et al., 2018; Luo & Lau, 2019; Yang et al., 2017) even in the absence/presence of absolute UDI/UMI. However, the influence of limited evapotranspiration on humidity in cities, caused by impervious landcover, is best shown during daytime due to the absence of UHI and higher evapotranspiration rates. Daytime absolute UDI as well as higher absolute UDI in summer than winter suggest that evapotranspiration differences between urban and rural areas are very likely causing such an absolute UDI (see also Hao et al., 2018).

4.2 UDI and outlook on potential impacts on human health, energy usage and urban ecology

In contrast to UHIs (e.g. Manoli et al., 2019; Venter et al., 2021), large scale studies quantifying diurnal and seasonal patterns of UDI and UMI magnitudes have been absent even though altered humidity in cities can similarly impact human health, building energy consumption, and urban ecology.

Heat stress is influenced by both temperature and humidity (Coffel et al., 2018; Mora et al., 2017) and especially, in hot and humid regions, an increase in humidity can decrease the outdoor thermal comfort (OTC) (Chow et al., 2016; Meili, Acero, et al., 2021). While urbanization increases UHI (K. Huang et al., 2019), the concurrent intensification of the UDI was found to offset some of the anticipated increase in hot and humid heat stress in summer in Beijing (X. Wang & Gong, 2010). On

the other hand, a large-scale increase in irrigation, albeit not in cities, has been shown to enhance moist heat stress extremes in India due to the increase in humidity (Mishra et al., 2020). Studies like these show that not just high temperatures and UHI but also humidity and UDI can impact outdoor thermal comfort, heat stress, and consequently human health. Hence, further studies are required to systematically quantify the effects of the observed magnitude of UDI reported here on heat stress, which could be especially relevant as UDI are largest during the warm season and daytime (Figure 3 and 4), when heat mitigation is mostly needed.

Heat mitigation strategies, such as urban greenery, influence both UHI and UDI. Increasing humidity due to plant evapotranspiration could limit the improvement in outdoor thermal comfort associated with urban vegetation (Hass et al., 2016; Meili, Acero, et al., 2021). At the same time, high VPD, likely exacerbated by UDI in cities, can impact plant stomatal response (Chen et al., 2011; Gillner et al., 2017; Novick et al., 2016; Winbourne et al., 2020) potentially limiting the evpotranspirative cooling potential of urban vegetation during periods of intense heat (Meili, Manoli, et al., 2021). These counteracting processes of reduced evapotranspiration due to stomatal closure at times of high VPD and the general increase in humidity by evapotranspiration in cities during normal VPD conditions are often neglected in studies predicting vegetation effects on urban climate. Only few urban microclimate models include detailed vegetation formulations (e.g. Meili et al., 2020; Nice et al., 2018) and further measurements and modelling studies are needed to understand the complex interaction between urban humidity, plant transpiration, and vegetation benefits during heatwaves.

Higher temperatures in cities can also lead to an increase in building energy demand for cooling (Santamouris, 2014). Recent studies have shown that making predictions based on air temperature alone without the consideration of humidity can lead to an underprediction of up to 10-15% of present and future building cooling demand (Maia-Silva et al., 2020). In hot and humid regions, Fonseca & Schlueter (2020) found that the increase in energy usage for building cooling is largely driven by higher needs for dehumidification rather than cooling itself. This is of special importance as tropical and sub-tropical cities have a large potential for an increase in energy usage for cooling in the future (Waite et al., 2017). Due to the impact of humidity on the quantification of building energy cooling demand, UDI and UMI magnitudes thus require careful evaluation, and their impacts need to be considered in future studies.

4.3 Limits of interpretation

The UDI and UHI magnitudes calculated in this study are averages over many cities and hence, depend on the ensemble of stations used. As most of the rural and urban meteorological stations are located in the northern mid-latitudes, the trends observed here are representing predominantly UDI and UHI magnitudes of mid-latitude cities in North America, Europe, and Asia. As discussed, humidity can have a large impact on moist heat stress and on energy usage for dehumidification in hot and humid regions, which suggests studies characterizing the urban humidity environment and UDI in tropical cities are urgently needed. To analyze possible differences in UDI due to background aridity, we analyzed trends for stations with WI<1 (water limited) and WI>1 (energy limited), separately. However, the results (SI Figure 16) are highly dependent on the chosen WI cut-off point and hence are not very robust. Furthermore, urbanization is approximated in this study by the increase in artificial impervious areas without consideration of city structure and urban fabric, number of inhabitants or other site-specific characteristics, which could affect the magnitude of UHI and UDI. However, due to the very large number of stations used, our approach is expected to average out many of these city-level differences and provide an “average” estimate of UDI magnitude and patterns.

While the land surface scheme used in the construction of the ERA5 reanalysis product does currently not simulate urban areas (Balsamo et al., 2009; Bassett et al., 2021; Hogan et al., 2017; Venter et al., 2021), the ERA5 product could still include implicitly urbanization due to air temperature assimilation from weather stations. However, such effects have been found to be negligible in a study quantifying UHI trends in London with the use of ERA5 (Bassett et al., 2021).

As the increase in artificial impervious area is quantified within a radius of 7 km around each meteorological station, the reported results are representative of the large-scale urbanization effect on the atmospheric conditions and thus of mesoscale UDI and UHI changes. This means that the results do not represent the effects of small scale-land cover change (e.g., a local parking lot, increase in building heights, construction of a pond) on local microclimate, which might exist in some of the analyzed stations. We further would like to highlight, that while the diurnal and seasonal patterns presented in this study do not change with changing buffer radius in the range of 2 – 9 km, the absolute magnitude of UHI and UDI is dependent on the selected buffer radius as urbanization rates tend to decrease at higher buffer radii (SI Figure 3). Magnitude of diurnal and seasonal patterns of UHI and UDI calculated for a 4 km and a 9 km buffer radius are shown in the supplementary information (SI Figure 4-7). Further note that the horizontal extent of urban temperature effects can extend beyond the city boundary (Fan et al., 2017) and hence, some stations could also be influenced by adjacent regions with large land conversion rates. Last, in our analysis, a fully urbanized area not undergoing any landcover change during the study period has an urbanization rate of zero equal to a natural area not undergoing urbanization. We also assume that the relationship between urbanization and the formation of UHI and UDI is linear and that there is no interaction between the absolute fraction of impervious urban land cover and the climate change signal. However, rural and urban stations could respond differently to an overall changing climate as Li & Bou-Zeid (2013) have shown that there could be a synergistic interaction between UHI and heat waves increasing temperatures in cities beyond the simple sum of the UHI and the heat wave signal. While we expect some of these limitations to affect the magnitude of the computed UHI and UDI, the seasonal and diurnal patterns are much more robust as shown by the sensitivity analysis to the buffer radius.

5. Conclusions

In contrast to UHI, investigations of UDI are scarce and confined to case-studies of single cities or urbanizing regions. However, UDI could potentially affect thermal comfort and human well-being, building energy consumption, and urban ecology. Large scale global analyses of UHI and UDI are often limited by meteorological data availability as concurrent measurements within cities and their surrounding rural areas are unavailable at the global scale. To overcome this limitation, we leverage the fact that many regions experienced rapid urbanization in the last few decades, which led to the development and intensification of UHI and UDI effects.

Our global scale analysis shows that absolute UDI is largest during daytime with a peak in the late afternoon and early evening hours. In contrast, relative UDI is largest during nighttime peaking in the late evening hours in summer. Generally, absolute and relative UDI are largest during the warm season and much smaller during winter, with the exception of daytime UDI_{RH}, which does not show a distinct seasonal pattern. UDI_{RH} exhibits a stronger diurnal pattern than UDI_{VPD}. Our analysis recovers typically observed diurnal UHI patterns showing higher temperatures during nighttime and the absence of UHI during day. UHI is larger during the warm season and negligible during winter, a pattern also found in large scale studies on surface UHI (Manoli et al., 2020b; Paschalis et al., 2021; Zhou et al., 2013). We further show that the distinction between relative and absolute UDI and their diurnal and seasonal patterns is fundamental to reconcile differences in the UDI literature. In summary, urbanization

induced humidity changes might be as relevant as temperature changes and are statistically much more evident. The global magnitude and patterns of absolute and relative UDI reported in this study represent a starting point for quantification of humidity effects on outdoor thermal comfort, building energy consumption, and urban ecology.

Acknowledgement

NM and SF acknowledges the support of the National University of Singapore through the project ''Bridging scales from below: The role of heterogeneities in the global water and carbon budgets'' Award Number: 22-3637-A0001. GM acknowledges support by ``The Branco Weiss Fellowship - Society in Science" administered by ETH Zurich.

Declaration of competing interest

The authors declare that they have no known competing financial interests or personal relationships that could have appeared to influence the work reported in this paper.

Data availability

The data that support the findings of this study are openly available.

Global Artificial Impervious Areas (GAIA) at 30 m resolution (Gong et al., 2020) were downloaded from http://data.ess.tsinghua.edu.cn, 22nd of March 2021.

HadISD version 3.1.1.2020f data were obtained from http://www.metoffice.gov.uk/hadobs/hadisd on 1.6.2021 and are British Crown Copyright, Met Office provided under an Open Government License, http://www.nationalarchives.gov.uk/doc/non-commercial--government-licence/non-commercial-government-licence.htm.

Cuchi., (2020) was downloaded from the Copernicus Climate Change Service (C3S) Climate Data Store.

Bibliography

Ackerman, B. (1987). Climatology of Chicago Area Urban–Rural Differences in Humidity. *Journal of Climate and Applied Meteorology*, *26*(3), 427–430.

Balsamo, G., Viterbo, P., Beijaars, A., van den Hurk, B., Hirschi, M., Betts, A. K., & Scipal, K. (2009). A revised hydrology for the ECMWF model: Verification from field site to terrestrial water storage and impact in the integrated forecast system. *Journal of Hydrometeorology*, *10*(3), 623–643. https://doi.org/10.1175/2008JHM1068.1

Bassett, R., Janes-Bassett, V., Phillipson, J., Young, P. J., & Blair, G. S. (2021). Climate driven trends in London's urban heat island intensity reconstructed over 70 years using a generalized additive model. *Urban Climate*, *40*(September), 100990. https://doi.org/10.1016/j.uclim.2021.100990

Chen, L., Zhang, Z., Li, Z., Tang, J., Caldwell, P., & Zhang, W. (2011). Biophysical control of whole tree transpiration under an urban environment in Northern China. *Journal of Hydrology*, *402*(3–4), 388–400. https://doi.org/10.1016/j.jhydrol.2011.03.034

Chow, W. T. L., Akbar, S. N. A. B. A., Heng, S. L., & Roth, M. (2016). Assessment of measured and perceived microclimates within a tropical urban forest. *Urban Forestry and Urban Greening*, *16*, 62–75. https://doi.org/10.1016/j.ufug.2016.01.010

Climate Data Store. (2020). *Near surface meteorological variables from 1979 to 2018 derived from bias-corrected reanalysis*. https://doi.org/10.24381/cds.20d54e34

Coffel, E. D., Horton, R. M., & De Sherbinin, A. (2018). Temperature and humidity based projections of a rapid rise in global heat stress exposure during the 21st century. *Environmental Research Letters*, *13*(1). https://doi.org/10.1088/1748-9326/aaa00e

Cuadrat, J. M., Vicente-Serrano, S., & Saz, M. A. (2015). Influence of different factors on relative air humidity in Zaragoza, Spain. *Frontiers in Earth Science*, *3*(March), 1–8. https://doi.org/10.3389/feart.2015.00010

Cucchi, M., P. Weedon, G., Amici, A., Bellouin, N., Lange, S., Müller Schmied, H., Hersbach, H., & Buontempo, C. (2020). WFDE5: Bias-adjusted ERA5 reanalysis data for impact studies. *Earth System Science Data*, *12*(3), 2097–2120. https://doi.org/10.5194/essd-12-2097-2020

Du, R., Song, J., Huang, X., Wang, Q., Zhang, C., Brousse, O., & Chan, P. W. (2022). High-resolution regional modeling of urban moisture island: mechanisms and implications on thermal comfort. *Building and Environment*, *207*(November 2021). https://doi.org/10.1016/j.buildenv.2021.108542

Dunn, J. H. R., Willett, M. K., Parker, E. D., & Mitchell, L. (2016). Expanding HadISD: Quality-controlled, sub-daily station data from 1931. *Geoscientific Instrumentation, Methods and Data Systems*, *5*(2), 473–491. https://doi.org/10.5194/gi-5-473-2016

Dunn, R. J. H. (2019). *HadISD version 3: monthly updates, Hadley Centre Technical Note*.

Dunn, R. J. H., Willett, K. M., Morice, C. P., & Parker, D. E. (2014). Pairwise homogeneity assessment of HadISD. *Climate of the Past*, *10*(4), 1501–1522. https://doi.org/10.5194/cp-10-1501-2014

Dunn, R. J. H., Willett, K. M., Thorne, P. W., Woolley, E. V., Durre, I., Dai, A., Parker, D. E., & Vose, R. S. (2012). HadISD: A quality-controlled global synoptic report database for selected variables at long-term stations from 1973-2011. *Climate of the Past*, *8*(5), 1649–1679. https://doi.org/10.5194/cp-8-1649-2012

Fan, Y., Li, Y., Bejan, A., Wang, Y., & Yang, X. (2017). Horizontal extent of the urban heat dome flow. *Scientific Reports*, *7*(1), 1–10. https://doi.org/10.1038/s41598-017-09917-4

Fonseca, J., & Schlueter, A. (2020). Daily enthalpy gradients and the effects of climate change on the thermal energy demand of buildings in the United States. *Applied Energy*, *262*(September 2019), 114458. https://doi.org/10.1016/j.apenergy.2019.114458

Fortuniak, K., Kłysik, K., & Wibig, J. (2006). Urban - Rural contrasts of meteorological parameters in Łódź. *Theoretical and Applied Climatology*, *84*(1–3), 91–101. https://doi.org/10.1007/s00704-005-0147-y

Gillner, S., Korn, S., Hofmann, M., & Roloff, A. (2017). Contrasting strategies for tree species to cope with heat and dry conditions at urban sites. *Urban Ecosystems*, *20*(4), 853–865. https://doi.org/10.1007/s11252-016-0636-z

Gong, P., Li, X., Wang, J., Bai, Y., Chen, B., Hu, T., Liu, X., Xu, B., Yang, J., Zhang, W., & Zhou, Y. (2020). Annual maps of global artificial impervious area (GAIA) between 1985 and 2018. *Remote Sensing of Environment*, *236*(August 2019), 111510. https://doi.org/10.1016/j.rse.2019.111510

Hage, K. D. (1975). Urban-Rural Humidity Differences. *Journal of Applied Meteorology*, *14*.

Hao, L., Huang, X., Qin, M., Liu, Y., Li, W., & Sun, G. (2018). Ecohydrological Processes Explain Urban Dry Island Effects in a Wet Region, Southern China. *Water Resources Research*, *54*(9), 6757–6771. https://doi.org/10.1029/2018WR023002

Harris, I., Osborn, T. J., Jones, P., & Lister, D. (2020). Version 4 of the CRU TS monthly high-resolution gridded multivariate climate dataset. *Scientific Data*, *7*(1), 1–18.

https://doi.org/10.1038/s41597-020-0453-3

Hass, A. L., Ellis, K. N., Mason, L. R., Hathaway, J. M., & Howe, D. A. (2016). Heat and humidity in the city: Neighborhood heat index variability in a mid-sized city in the Southeastern United States. *International Journal of Environmental Research and Public Health*, *13*(1). https://doi.org/10.3390/ijerph13010117

Hersbach, H., Bell, B., Berrisford, P., Hirahara, S., Horányi, A., Muñoz-Sabater, J., Nicolas, J., Peubey, C., Radu, R., Schepers, D., Simmons, A., Soci, C., Abdalla, S., Abellan, X., Balsamo, G., Bechtold, P., Biavati, G., Bidlot, J., Bonavita, M., … Thépaut, J. N. (2020). The ERA5 global reanalysis. *Quarterly Journal of the Royal Meteorological Society*, *146*(730), 1999–2049. https://doi.org/10.1002/qj.3803

Hogan, R. J., Ahlgrimm, M., Balsamo, G., Beljaars, A., Bozzo, A., Di, F., Forbes, R. M., Lang, S., Mayer, M., Sandu, I., Vitart, F., & Wedi, N. (2017). *Radiation in numerical weather prediction* (Issue October).

Huang, K., Li, X., Liu, X., & Seto, K. C. (2019). Projecting global urban land expansion and heat island intensification through 2050. *Environmental Research Letters*, *14*(11). https://doi.org/10.1088/1748-9326/ab4b71

Huang, X., Song, J., Wang, C., Chui, T. F. M., & Chan, P. W. (2021). The synergistic effect of urban heat and moisture islands in a compact high-rise city. *Building and Environment*, *205*(August). https://doi.org/10.1016/j.buildenv.2021.108274

Kuttler, W., Weber, S., Schonnefeld, J., & Hesselschwerdt, A. (2007). Urban/rural atmospheric water vapour pressure differences and urban moisture excess in Krefeld, Germany. *International Journal of Climatology*, *2029*(April 2007), 2005–2015. https://doi.org/10.1002/joc

Langendijk, G. S., Rechid, D., & Jacob, D. (2019). Urban areas and urban-rural contrasts under climate change: What does the EURO-CORDEX ensemble tell us?-Investigating near surface humidity in berlin and its surroundings. *Atmosphere*, *10*(12). https://doi.org/10.3390/ATMOS10120730

Lee, D. O. (1991). Urban—rural humidity differences in London. *International Journal of Climatology*, *11*(5), 577–582. https://doi.org/10.1002/joc.3370110509

Li, D., & Bou-Zeid, E. (2013). Synergistic Interactions between Urban Heat Islands and Heat Waves : The Impact in Cities Is Larger than the Sum of Its Parts *. *Journal of Applied Meteorology and Climatology*, *52*, 2051–2064. https://doi.org/10.1175/JAMC-D-13-02.1

Li, X., Li, W., Middel, A., Harlan, S. L., Brazel, A. J., & Turner, B. L. (2016). Remote sensing of the surface urban heat island and land architecture in Phoenix, Arizona: Combined effects of land composition and configuration and cadastral-demographic-economic factors. *Remote Sensing of Environment*, *174*, 233–243. https://doi.org/10.1016/j.rse.2015.12.022

Li, Y., Schubert, S., Kropp, J. P., & Rybski, D. (2020). On the influence of density and morphology on the Urban Heat Island intensity. *Nature Communications*, *11*(1), 1–9. https://doi.org/10.1038/s41467-020-16461-9

Lokoshchenko, M. A. (2017). Urban heat island and urban dry island in Moscow and their centennial changes. *Journal of Applied Meteorology and Climatology*, *56*(10), 2729–2745. https://doi.org/10.1175/JAMC-D-16-0383.1

Luo, M., & Lau, N. C. (2019). Urban Expansion and Drying Climate in an Urban Agglomeration of East China. *Geophysical Research Letters*, *46*(12), 6868–6877. https://doi.org/10.1029/2019GL082736

Maia-Silva, D., Kumar, R., & Nateghi, R. (2020). The critical role of humidity in modeling summer electricity demand across the United States. *Nature Communications*, *11*(1), 1–8. https://doi.org/10.1038/s41467-020-15393-8

Manoli, G., Fatichi, S., Bou-Zeid, E., & Katul, G. G. (2020a). Seasonal hysteresis of surface urban heat islands. *Proceedings of the National Academy of Sciences*, *117*(13), 7082–7089. https://doi.org/10.1073/pnas.1917554117

Manoli, G., Fatichi, S., Bou-Zeid, E., & Katul, G. G. (2020b). Seasonal hysteresis of surface urban heat islands. *Proceedings of the National Academy of Sciences of the United States of America*, *117*(13), 7082–7089. https://doi.org/10.1073/pnas.1917554117

Manoli, G., Fatichi, S., Schläpfer, M., Yu, K., Crowther, T. W., Meili, N., Burlando, P., Katul, G. G., & Bou-Zeid, E. (2019). Magnitude of urban heat islands largely explained by climate and population. *Nature*, *573*(7772), 55–60. https://doi.org/10.1038/s41586-019-1512-9

Meili, N., Acero, J. A., Peleg, N., Manoli, G., Burlando, P., & Fatichi, S. (2021). Vegetation cover and plant-trait effects on outdoor thermal comfort in a tropical city. *Building and Environment*, *195*(September 2020), 107733. https://doi.org/10.1016/j.buildenv.2021.107733

Meili, N., Manoli, G., Burlando, P., Bou-Zeid, E., Chow, W. T., Coutts, A., Daly, E., Nice, K., Roth, M., Tapper, N., Velasco, E., Vivoni, E., & Fatichi, S. (2020). An urban ecohydrological model to quantify the effect of vegetation on urban climate and hydrology (UT&C v1.0). *Geoscientific Model Development*, *13*, 335–362. https://doi.org/10.5194/gmd-2019-225

Meili, N., Manoli, G., Burlando, P., Carmeliet, J., Chow, W. T. L., Coutts, A. M., Roth, M., Velasco, E., Vivoni, E. R., & Fatichi, S. (2021). Tree effects on urban microclimate: diurnal, seasonal, and climatic temperature differences explained by separating radiation, evapotranspiration, and roughness effects. *Urban Forestry & Urban Greening*, *58*, 126970. https://doi.org/10.1016/j.ufug.2020.126970

Mishra, V., Ambika, A. K., Asoka, A., Aadhar, S., Buzan, J., Kumar, R., & Huber, M. (2020). Moist heat stress extremes in India enhanced by irrigation. *Nature Geoscience*, *13*(11), 722–728. https://doi.org/10.1038/s41561-020-00650-8

Mora, C., Dousset, B., Caldwell, I. R., Powell, F. E., Geronimo, R. C., Bielecki, C. R., Counsell, C. W. W., Dietrich, B. S., Johnston, E. T., Louis, L. V, Lucas, M. P., Mckenzie, M. M., Shea, A. G., Tseng, H., Giambelluca, T. W., Leon, L. R., Hawkins, E., & Trauernicht, C. (2017). Global risk of deadly heat. *Nature Climate Change*, *June*. https://doi.org/10.1038/NCLIMATE3322

Moriwaki, R., Watanabe, K., & Morimoto, K. (2013). Urban Dry Island Phenomenon and Its Impact on Cloud Base Level. *Journal of JSCE*, *1*(1), 521–529. https://doi.org/10.2208/journalofjsce.1.1_521

Moustakis, Y., Onof, C. J., & Paschalis, A. (2020). Atmospheric convection, dynamics and topography shape the scaling pattern of hourly rainfall extremes with temperature globally. *Communications Earth & Environment*, *1*(1), 1–9. https://doi.org/10.1038/s43247-020-0003-0

Moustakis, Y., Papalexiou, S. M., Onof, C. J., & Paschalis, A. (2021). Seasonality, Intensity, and Duration of Rainfall Extremes Change in a Warmer Climate. *Earth's Future*, *9*(3), 1–15. https://doi.org/10.1029/2020EF001824

Nice, K. A., Coutts, A. M., & Tapper, N. J. (2018). Development of the VTUF-3D v1.0 urban micro-climate model to support assessment of urban vegetation influences on human thermal comfort. *Urban Climate*, 1–25. https://doi.org/10.1016/j.uclim.2017.12.008

Novick, K. A., Ficklin, D. L., Stoy, P. C., Williams, C. A., Bohrer, G., Oishi, A. C., Papuga, S. A., Blanken, P. D., Noormets, A., Sulman, B. N., Scott, R. L., Wang, L., & Phillips, R. P. (2016). The increasing

importance of atmospheric demand for ecosystem water and carbon fluxes. *Nature Climate Change*, *6*(11), 1023–1027. https://doi.org/10.1038/nclimate3114

Oke, T. R., Mills, G., Christen, A., & Voogt, J. A. (2017). *Urban climates*. Cambridge University Press. https://doi.org/10.1016/s0168-6321(06)80036-2

Paschalis, A., Chakraborty, T., Fatichi, S., Meili, N., & Manoli, G. (2021). Urban Forests as Main Regulator of the Evaporative Cooling Effect in Cities. *AGU Advances*, *2*(2). https://doi.org/10.1029/2020av000303

Peng, S., Piao, S., Ciais, P., Friedlingstein, P., & Ottle, C. (2011). *Surface Urban Heat Island Across 419 Global Big Cities Surface Urban Heat Island Across 419 Global Big Cities*. *October 2016*. https://doi.org/10.1021/es2030438

Santamouris, M. (2014). On the energy impact of urban heat island and global warming on buildings. *Energy and Buildings*, *82*, 100–113. https://doi.org/10.1016/j.enbuild.2014.07.022

Shuttleworth, W. J. (2012). *Terrestrial hydrometeorology*. John Wiley & Sons, Ltd.

Smith, A., Lott, N., & Vose, R. (2011). The integrated surface database: Recent developments and partnerships. *Bulletin of the American Meteorological Society*, *92*(6), 704–708. https://doi.org/10.1175/2011BAMS3015.1

Tapper, N. J. (1990). Urban influences on boundary layer temperature and humidity: Results from Christchurch, New Zealand. *Atmospheric Environment*, *24*(1), 19–27. https://doi.org/10.1016/0957-1272(90)90005-F

Tuholske, C., Caylor, K., Funk, C., Verdin, A., Sweeney, S., Grace, K., Peterson, P., & Evans, T. (2021). Global urban population exposure to extreme heat. *Proceedings of the National Academy of Sciences of the United States of America*, *118*(41), 1–9. https://doi.org/10.1073/pnas.2024792118

United Nations. (2018). The World ’s Cities in 2018. In *The World’s Cities in 2018 - Data Booklet (ST/ESA/ SER.A/417)*.

Venter, Z. S., Chakraborty, T., & Lee, X. (2021). Crowdsourced air temperatures contrast satellite measures of the urban heat island and its mechanisms. *Science Advances*, *7*(22), 1–10. https://doi.org/10.1126/sciadv.abb9569

Waite, M., Cohen, E., Torbey, H., Piccirilli, M., Tian, Y., & Modi, V. (2017). Global trends in urban electricity demands for cooling and heating. *Energy*, *127*, 786–802. https://doi.org/10.1016/j.energy.2017.03.095

Wang, C., Myint, S. W., Wang, Z., & Song, J. (2016). Spatio-temporal modeling of the urban heat island in the Phoenix metropolitan area: Land use change implications. *Remote Sensing*, *8*(3). https://doi.org/10.3390/rs8030185

Wang, X., & Gong, Y. (2010). The impact of an urban dry island on the summer heat wave and sultry weather in Beijing City. *Chinese Science Bulletin*, *55*, 1657–1661. https://doi.org/https://doi-org.libproxy1.nus.edu.sg/10.1007/s11434-010-3088-5

Wang, Z., Song, J., Chan, P. W., & Li, Y. (2021). The urban moisture island phenomenon and its mechanisms in a high-rise high-density city. *International Journal of Climatology*, *41*(S1), E150–E170. https://doi.org/10.1002/joc.6672

Ward, K., Lauf, S., Kleinschmit, B., & Endlicher, W. (2016). Heat waves and urban heat islands in Europe : A review of relevant drivers. *Science of the Total Environment, The*, *569–570*, 527–539. https://doi.org/10.1016/j.scitotenv.2016.06.119

Warren, E. L., Young, D. T., Chapman, L., Muller, C., Grimmond, C. S. B., & Cai, X. M. (2016). The Birmingham Urban Climate Laboratory-A high density, urban meteorological dataset, from 2012-2014. *Scientific Data*, *3*, 1–8. https://doi.org/10.1038/sdata.2016.38

Winbourne, J. B., Jones, T. S., Garvey, S. M., Harrison, J. L., Wang, L., Li, D., Templer, P. H., & Hutyra, L. R. (2020). Tree transpiration and urban temperatures: Current understanding, implications, and future research directions. *BioScience*, *70*(7), 576–588. https://doi.org/10.1093/biosci/biaa055

Yang, P., Ren, G., & Hou, W. (2017). Temporal-spatial patterns of relative humidity and the urban dryness island effect in Beijing City. *Journal of Applied Meteorology and Climatology*, *56*(8), 2221–2237. https://doi.org/10.1175/JAMC-D-16-0338.1

Zhao, L., Lee, X., Smith, R. B., & Oleson, K. (2014). Strong contributions of local background climate to urban heat islands. *Nature*, *511*(7508), 216–219. https://doi.org/10.1038/nature13462

Zhou, B., Rybski, D., & Kropp, J. P. (2013). On the statistics of urban heat island intensity. *Geophysical Research Letters*, *40*(20), 5486–5491. https://doi.org/10.1002/2013GL057320